

Changes in the tropical lapse rate due to entrainment and their impact on climate sensitivity

Jiawei Bao¹, Bjorn Stevens², Lukas Kluft², and Diego Jiménez de la Cuesta Otero²

¹Max Planck Institute for Meteorology

²Max Planck Institute for Meteorology

November 21, 2022

Abstract

The tropical temperature in the free troposphere deviates from a theoretical moist-adiabat. The overall deviations are attributed to entrainment of dry surrounding air. The deviations gradually approach zero in the upper troposphere, which we explain with a buoyancy-sorting mechanism: the height to which individual convective parcels rise depends on parcel buoyancy, which is closely tied to the impact of entrainment during ascent. In higher altitudes, the temperature is increasingly controlled by the convective parcels that are warmer and more buoyant, because of weaker entrainment effects. We represent such temperature deviations from moist-adiabats in a clear-sky one-dimensional radiative-convective equilibrium model. Compared with a moist-adiabatic adjustment, having the entrainment-induced temperature deviations leads to higher climate sensitivity. As the impact of entrainment depends on the saturation deficit which increases with warming, our model predicts even more amplified surface warming from entrainment in a warmer climate.

1 **Changes in the tropical lapse rate due to entrainment**
2 **and their impact on climate sensitivity**

3 **Jiawei Bao¹, Bjorn Stevens¹, Lukas Kluft¹, Diego Jiménez-de-la-Cuesta¹**

4 ¹Max Planck Institute for Meteorology, Hamburg, Germany

5 **Key Points:**

- 6 • The tropical temperature profile in the free troposphere deviates from that fol-
7 lowing a moist-adiabatic lapse rate.
8 • The deviations from the moist-adiabatic lapse rate can be explained by entrain-
9 ment with a buoyancy-sorting mechanism.
10 • The temperature deviations from moist-adiabats increase climate sensitivity.

Corresponding author: Jiawei Bao, jiawei.bao@mpimet.mpg.de

Abstract

The tropical temperature in the free troposphere deviates from a theoretical moist-adiabat. The overall deviations are attributed to entrainment of dry surrounding air. The deviations gradually approach zero in the upper troposphere, which we explain with a buoyancy-sorting mechanism: the height to which individual convective parcels rise depends on parcel buoyancy, which is closely tied to the impact of entrainment during ascent. In higher altitudes, the temperature is increasingly controlled by the convective parcels that are warmer and more buoyant, because of weaker entrainment effects. We represent such temperature deviations from moist-adiabats in a clear-sky one-dimensional radiative-convective equilibrium model. Compared with a moist-adiabatic adjustment, having the entrainment-induced temperature deviations leads to higher climate sensitivity. As the impact of entrainment depends on the saturation deficit which increases with warming, our model predicts even more amplified surface warming from entrainment in a warmer climate.

Plain Language Summary

The tropical temperature structure is determined by regions with deep convection, which is believed to be moist-adiabatic. However, both models and observations show that the temperature deviates from moist-adiabats. This is because convective parcels often mix with dry environmental air during ascent, pushing the temperature away from the moist-adiabatic structure. More importantly, the tropical temperature is not dominated by one or a few strongest convective plumes, but rather controlled by the combined effect of many convective plumes of different strengths and depths. Therefore, the tropical temperature structure reflects the composition of convection happening at different values of boundary-layer energy and mixing processes of variable efficiency with the environment. Using an idealized model, we find that representing such a deviation in the temperature structure increases the surface warming, because the resulting temperature lapse rate is more similar to a constant lapse rate, showing less temperature increase higher up than a moist-adiabatic lapse rate. This effect is likely amplified in a warmer climate due to this mixing process becoming more efficient in pushing the temperature further away from moist-adiabats.

1 Introduction

A moist-adiabatic process describes when a moist air parcel ascends, it cools as it expands and condenses due to saturation. By releasing the fusion enthalpy, condensation acts to partially compensate the cooling due to expansion. The whole process occurs adiabatically without exchanging heat with the environment. The temperature lapse rate of an air parcel that undergoes this undiluted ascent process is a moist-adiabatic lapse rate. The temperature in the tropical free troposphere is generally believed to follow a moist-adiabatic lapse rate, because gravity waves generated by deep convection rapidly homogenizes the horizontal buoyancy anomaly so as to adjust the density temperature in the non-convecting regions to that in the convecting regions (Bretherton & Smolarkiewicz, 1989; Mapes, 1993; Sobel & Bretherton, 2000). Therefore, the free-tropospheric temperature in the tropics is set by the regions with deep convection. The key element in the moist-adiabatic definition is that the entire process does not exchange heat with the environment, which is rather something too ambitious to achieve in a realistic context. Still, the moist-adiabatic temperature structure in the tropical atmosphere is supported by some observational studies (Betts, 1986; Xu & Emanuel, 1989).

One idea that goes against a moist-adiabatic thermal structure is that the tropical temperature may not be determined by one or a few strongest convective plumes, but rather by the mean effect from all convection occurring. As a result, to stay moist-adiabatic throughout the entire free troposphere, the mean convection, consisting of numerous convective parcels, has to be moist-adiabatic. This is an unrealistic idea, because

61 already the convection that undergoes moist-adiabatic ascent is extremely rare (Romps
 62 & Kuang, 2010). Studies using storm-resolving simulations (SRMs) in idealized config-
 63 uration of radiative-convective equilibrium (RCE) show that the tropical temperature
 64 tends to deviate from moist-adiabats, because the saturated convective air parcels of-
 65 ten mix with the unsaturated environmental air, a process which is referred to as entrain-
 66 ment (Singh & O’Gorman, 2013, 2015; Seeley & Romps, 2015). Entrainment reduces the
 67 temperature by pushing the convective air parcels away from the original moist-adiabatic
 68 trajectories. These results suggest that the assumption of a moist-adiabatic structure
 69 of tropical temperature may be too simplistic.

70 To what extent does the tropospheric temperature obey the moist-adiabatic lapse
 71 rate? The answer is central to understanding some of the fundamental questions of cli-
 72 mate change. The vertical structure of atmospheric warming matters for radiation in two
 73 ways: it directly controls the thermal emission of an atmospheric layer, and limits the
 74 abundance of water vapor through its saturation value which varies with temperature.
 75 These are particularly important for the radiative response to warming which is often
 76 quantified by the lapse-rate and water vapor feedbacks. For a moist-adiabatic thermal
 77 structure, the enhanced tropospheric warming aloft relative to the surface allows more
 78 longwave emission to space than would be the case for a constant lapse rate, enabling
 79 a cooler surface temperature: a negative feedback. However, this negative lapse-rate feed-
 80 back is largely counteracted by the corresponding increase of water vapor following roughly
 81 the Clausius-Clapeyron relation (Soden & Held, 2006). More water vapor reduces emis-
 82 sivity, leading to warmer surface temperatures: a positive feedback. Changes in this sub-
 83 tle balance between the negative lapse-rate feedback and positive water vapor feedback
 84 can strongly affect the net feedback, leading to contrasting changes in the equilibrium
 85 climate sensitivity (ECS), which is defined as the steady-state temperature increase due
 86 to a doubling of the atmospheric CO₂ concentration. It has been shown that the same
 87 fractional increase of water vapor at different height alters the net feedback, leading to
 88 large changes in ECS (Soden & Held, 2006; Bourdin et al., 2021). Thus, a small depart-
 89 ure from the moist-adiabatic structure can potentially have a large impact on the ECS
 90 as well.

91 In this study, we look at the vertical temperature structure and seek to better un-
 92 derstand the deviations from moist-adiabats. For simplicity, the moist-adiabatic calcu-
 93 lation in this study adopts the pseudo-adiabatic formula as used in Bao and Stevens (2021).
 94 Furthermore, we investigate the impact of such temperature deviations on climate sen-
 95 sitivity. The climate sensitivity that we focus on is the clear-sky part of ECS, which we
 96 refer to as the clear-sky climate sensitivity (\mathcal{S}). We first look into the tropical lapse rate
 97 by analyzing the data from a global storm-resolving model. Then a simple hypothesis
 98 is proposed to explain the variations in the lapse rate by entrainment of dry environmen-
 99 tal air. Based on this hypothesis, we represent the new temperature profile by taking into
 100 account the temperature deviations from moist-adiabats in a one-dimensional clear-sky
 101 RCE model—konrad. Finally, we use this model to quantify the impact of temperature
 102 deviations from moist-adiabats on \mathcal{S} .

103 2 Modeling convection

104 2.1 Tropical temperature deviates from moist-adiabat due to the im- 105 pact of entrainment

106 We start by investigating the tropical temperature structure from a global storm-
 107 resolving model—ICON (ICOsahedral Non-hydrostatic model; Zängl et al., 2015; Hoheneg-
 108 ger et al., 2020). The model is configured to run at a quasi-uniform horizontal mesh of
 109 2.5 km for 40 days from August 1 in 2016. The data from the last ten days of the sim-
 110 ulations are used in the analysis. The initial conditions are from the global meteorolog-
 111 ical analysis at a grid spacing of 9.5 km from the European Center for Medium Range

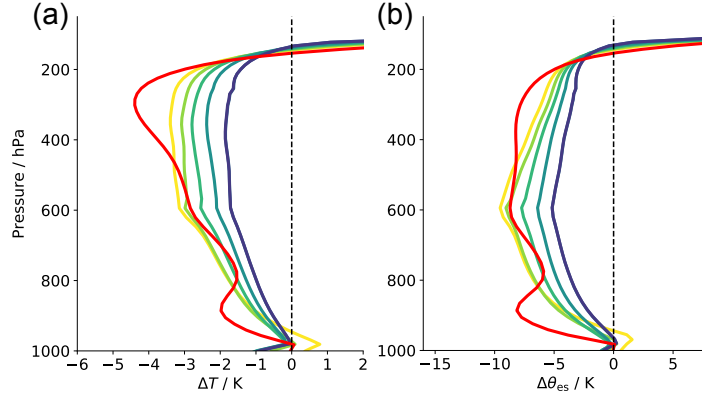


Figure 1. Differences in temperature (ΔT ; a) and saturation equivalent potential temperature ($\Delta\theta_{\text{es}}$; b) simulated by ICON relative to their corresponding moist-adiabatic profiles. Differences are shown for the tropic mean state (red) and the moist regions (colors from yellow to blue correspond to the 90th, 99th, 99.9th, 99.99th and 99.999th percentile of precipitable water).

112 Weather Forecasts (ECMWF) and the lower boundary conditions are daily observed sea
 113 surface temperatures. Details about the model setup are provided by Hohenegger et al.
 114 (2020). Here we focus on the tropical ocean regions over 10°N – 10°S .

115 Figure 1a shows that the tropical temperature profile is substantially colder than
 116 the theoretical moist-adiabat, and this deviation is larger in dry regions where the im-
 117 pact of entrainment is increased. A similar picture is also seen with saturation equiv-
 118 alent potential temperature (θ_{es}). The largest deviation of θ_{es} occurs in the mid-troposphere
 119 (600 hPa). Above that, the deviation reduces with height. As θ_{es} is a constant for the
 120 moist-adiabatic conditions, Figure 1b shows that θ_{es} increases with height above 600 hPa
 121 in the ICON simulations.

122 Such deviation from the moist-adiabat has been attributed to entrainment in con-
 123 vective clouds of environmental air that is usually drier than the parcel itself. This tends
 124 to reduce the temperature and pushes the air parcel away from saturation. However, this
 125 entrainment effect can only explain the temperature reduction in the lower troposphere.
 126 It fails to explain why θ_{es} in relatively drier conditions increases above 600 hPa as shown
 127 in Fig. 1b. In fact, the increase in θ_{es} with decreasing pressure implies that the temper-
 128 ature in the free troposphere is not regulated by the warmest convection with the high-
 129 est θ_{es} . If it were so, then this warmest convection would essentially kill all other con-
 130 vection and set the thermal structure of the troposphere, and θ_{es} would at best stay ver-
 131 tically constant, which is not case as seen in Fig. 1b.

132 We hypothesize that the mean tropical thermal structure reflects the composition
 133 of convection happening at different values of boundary-layer equivalent potential tem-
 134 perature (θ_e) and mixing more or less with the environment while rising up, as the tem-
 135 perature in the free troposphere is not determined by the one or a few strongest (or warmest)
 136 convection, but rather by the mean convection, which represents a combined effect from
 137 all convection occurring over each height. This can be understood with Fig. 2. The trop-
 138 ical atmosphere is composed of numerous convective systems. While most convection can
 139 reach a relatively lower altitude, the chance of convection occurring at a higher altitude
 140 is smaller, and even less can survive up to the tropopause. In order for an air parcel to
 141 reach a relatively higher altitude, this parcel has to maintain its positive buoyancy rela-
 142 tive to the surrounding environment. Entraining the environmental air into the updraft

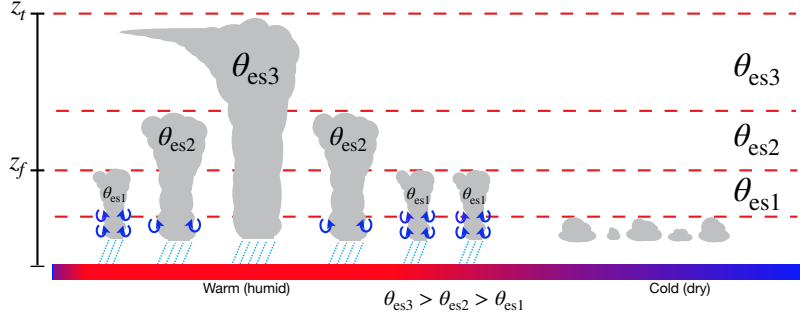


Figure 2. A schematic of tropical convection and temperature. Colors at the surface represents the sea surface temperature. Blue arrows represent the entrainment process. The height of the convective top is denoted by z_t . The freezing level is denoted by z_f .

143 would successively prevent the parcel from rising higher. As the height that each con-
 144 vective parcel can reach depends on the parcel buoyancy, the upper troposphere is in-
 145 creasingly dominated by the convective parcels that are warmer and more buoyant. These
 146 parcels usually arise in relatively more humid environment so that they can maintain the
 147 positive buoyancy. We refer to this height-dependence of parcel buoyancy as the buoy-
 148 ancancy sorting of convection. Thus, above a certain level where most air parcels cease to
 149 rise, θ_{es} increases with height as shown in Fig. 1b, because only the more buoyant air
 150 parcels with larger θ_{es} can continue rising up. This level appears to coincide with the
 151 freezing level, which is a stable layer as observed in Johnson et al. (1999) and tends to
 152 inhibit cloud growth and promote cloud detrainment (Stevens et al., 2017). The buoyancy-
 153 sorting mechanism is broadly consistent with a recent study by Zhou and Xie (2019) who
 154 proposed that the tropical mean temperature structure could not be represented by one
 155 convective plume, but rather by a spectral of plumes with different entrainment rates.

156 **2.2 Representing the temperature deviations from entrainment in kon-** 157 **rad**

158 We aim to represent the temperature profile that takes into account the deviation
 159 from the moist-adiabat in a clear-sky one-dimensional RCE model — konrad (Dacie et
 160 al., 2019; Kluft et al., 2019). In konrad, the original convective adjustment assumes that
 161 the temperature follows exactly a moist-adiabatic lapse rate, based on the surface tem-
 162 perature calculated by a slab-ocean model. To represent the temperature reduction from
 163 the impact of entrainment, we adopt the formula derived from the zero-buoyancy entrain-
 164 ing plume model by Singh and O’Gorman (2013). The simulated temperature profiles
 165 are compared with the tropical mean profile averaged over the period of 2006–2015 from
 166 the ERA5 reanalysis data (Hersbach et al., 2019).

167 Here we briefly review the main idea of the zero-buoyancy entraining plume model.
 168 The zero-buoyancy entraining plume assumes the cloud buoyancy is small. As the plume
 169 is saturated at the environment temperature above the cloud base, this allows us to de-
 170 rive the temperature reduction due to entrainment from the plume moist static energy
 171 (MSE) budget:

$$\frac{dh^*}{dz} = -\epsilon(h^* - h_e) = -\epsilon\ell_v(q_v^* - q_{ve}), \quad (1)$$

172 where ϵ is the entrainment rate, h^* is the saturated MSE at the environment temper-
 173 ature, h_e is the MSE of the environment, ℓ_v is the latent heat of evaporation, q_v^* is the

174 saturation specific humidity at the environment temperature, and q_{ve} is the specific hu-
 175 midity of the environment.

176 The MSE of an undiluted parcel (h_u) is conserved ($\frac{dh_u}{dz} = 0$). This makes the sat-
 177 uration MSE (h_u^*) above the cloud base also conserved such that $\frac{dh_u^*}{dz} = 0$. By subtract-
 178 ing Eq.(1), we get

$$\frac{d(h_u^* - h^*)}{dz} = \epsilon \ell_v (q_v^* - q_{ve}). \quad (2)$$

179 From Eq.(2), we integrate vertically to get the temperature reduction from the im-
 180 pact of entrainment (ΔT):

$$\Delta T(z) = \frac{1}{c_p + \ell_v \frac{\partial q_v^*}{\partial T}} \int_{z_b}^z \epsilon \ell_v (1 - RH) q_v^* dz', \quad (3)$$

181 where c_p is the isobaric specific heat capacity of the dry air, RH is the environmental
 182 relative humidity: $RH \simeq q_{ve}/q_v^*$, and z_b is the height of the cloud base. Equation (3)
 183 shows that the temperature reduction from the impact of entrainment depends on the
 184 entrainment rate as well as the saturation deficit. Following Romps (2014), RH is pre-
 185 dicted by temperature which exhibits a C shape and is roughly temperature invariant
 186 in the free troposphere (Fig. 3a). The results are qualitatively consistent if a constant
 187 RH profile is used. We use a fixed entrainment rate profile defined as $\epsilon(z) = \epsilon_0/z$ and
 188 ϵ_0 is the entrainment parameter. Because konrad uses pressure as its vertical coordinate,
 189 the variables simulated by konrad are converted from pressure to height assuming hy-
 190 drostatic balance before they are used in Eq. (3).

191 The temperature deviation term is not computed strictly from the entraining plume
 192 model. For simplicity, we utilize the formula (Eq. (3)) derived from the model and cal-
 193 culate the temperature deviation term directly. The final temperature profile is obtained
 194 by subtracting this temperature deviation term from the temperature assuming the moist-
 195 adiabatic adjustment. So we first calculate the moist-adiabatic temperature profile based
 196 on the surface temperature, and then use this temperature profile to compute q_v^* in Eq. (3).
 197 Although q_v^* corresponds to the saturation specific humidity of the environment, such
 198 a simplification would not qualitatively alter the results. Most importantly, the key im-
 199 pact of climate change, that is the Clausius-Clapeyron increase of q_v^* , is captured.

200 One major issue with the zero-buoyancy entraining plume model is that it assumes
 201 that the temperature in the free troposphere is controlled by the mean convection, but
 202 fails to represent the buoyancy sorting of convection. As a result, the upper-tropospheric
 203 temperature depicted by the model is unrealistic. Here to account for the reduced en-
 204 trainment effect with height, $\Delta T(z)$ in Eq. (3) is weighted by a coefficient $\xi(z)$ defined
 205 as:

$$\xi(z) = \begin{cases} \left(\frac{z - z_t}{z_b - z_t} \right)^{\frac{2}{3}}, & z_b \leq z \leq z_t \\ 0, & \text{elsewhere} \end{cases} \quad (4)$$

206 where z_t is the height at the convective top which is determined as the highest level to
 207 which convective adjustment is applied, and z_b is the cloud base height which, for sim-
 208 plicity, is kept at the height corresponding to a constant pressure of 960 hPa. $\xi(z)$ varies
 209 from 1 at the cloud base to 0 at the convective top, mimicking the reduced entrainment
 210 effect with increasing height. The exponent value is tuned so that the temperature de-
 211 viations are more realistic and Fig. 3b shows that our implementation by weighting the
 212 Eq. (3) with Eq. (4) reproduces similarly the characteristics of temperature deviations
 213 as those in ERA5.

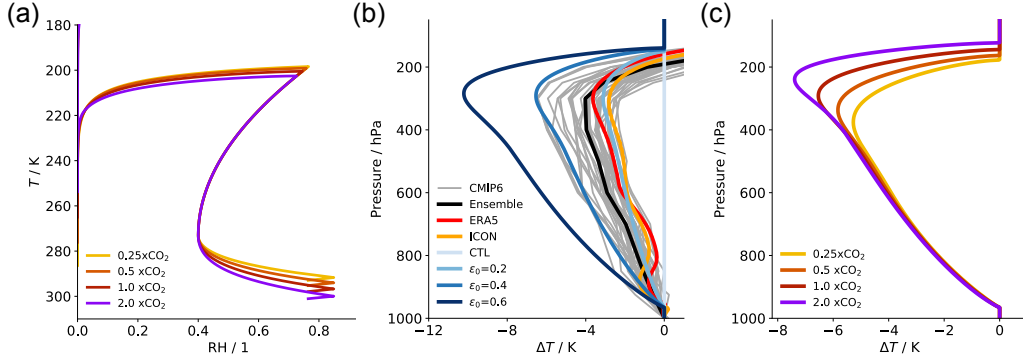


Figure 3. (a) Profiles of Relative humidity (RH) in temperature coordinates from the control (CTL) simulations with different CO₂ concentrations. (b) Profiles of temperature deviations (ΔT) from moist-adiabats from konrad simulations of $1\times\text{CO}_2$ with different entrainment parameter (ϵ_0), ERA5, ICON and CMIP6 (black line: multi-model ensemble; grey lines: individual models). (c) Profiles of temperature deviations (ΔT) from moist-adiabats from konrad simulations with different CO₂ concentrations and $\epsilon_0 = 0.4$.

214 We use konrad to quantify the impact of entrainment-induced deviations from moist-
 215 adiabat on the equilibrium surface temperature. Radiation is calculated using the RRTMG
 216 radiation scheme (Mlawer et al., 1997). The trace gas concentrations are consistent with
 217 those specified in the Radiative-Convective Equilibrium Model Intercomparison Project
 218 (RCEMIP; Wing et al., 2018). The default CO₂ concentration is 348 ppmv. First we run
 219 a simulation with the moist-adiabatic adjustment at a fixed SST of 298 K. The output
 220 from this simulation at the equilibrium state is used to initialize a set of experiments that
 221 is forced with a range of CO₂ concentrations from 0.25 to 2 times the default CO₂ con-
 222 centration. In these simulations, the heat sink of the slab ocean model is set to be the
 223 top-of-atmosphere net radiative flux of the fixed SST experiment. For each CO₂ con-
 224 centration, simulations are performed with two different convective adjustment options: the
 225 moist-adiabatic adjustment and the entrainment adjustment. The entrainment effect is
 226 investigated by varying the entrainment parameter ϵ_0 from 0.2 to 0.6. The simulations
 227 with the moist-adiabatic adjustment are the control experiments (CTL) and can be viewed
 228 as $\epsilon_0 = 0$. Additionally, to assist in interpretation, we run simulations with a fixed lapse
 229 rate of 6.5 K km^{-1} .

230 When estimating forcings and feedbacks, we want to compare simulations that only
 231 differ in their CO₂ concentrations. Therefore, each perturbed simulation is initialized with
 232 data from a simulation that uses the same configuration but the default CO₂ concen-
 233 tration. In this study, \mathcal{S} is calculated as the SST change from those simulations of a dou-
 234 bling of CO₂ relative to the initial SST. The forcing $\Delta F_{2\times\text{CO}_2}$ is the radiative imbalance
 235 per CO₂ doubling. Then the climate feedback parameter is defined as:

$$\lambda = -\frac{\Delta F_{2\times\text{CO}_2}}{\mathcal{S}}. \quad (5)$$

236 Here we obtain λ by regressing $\Delta F_{2\times\text{CO}_2}$ against ΔSST for each time step, following a
 237 method introduced by Gregory et al. (2004), and λ is given by the regression slope. It
 238 is worth noting that we are focusing on the clear-sky part of ECS, because all simula-
 239 tions are performed under clear-sky conditions.

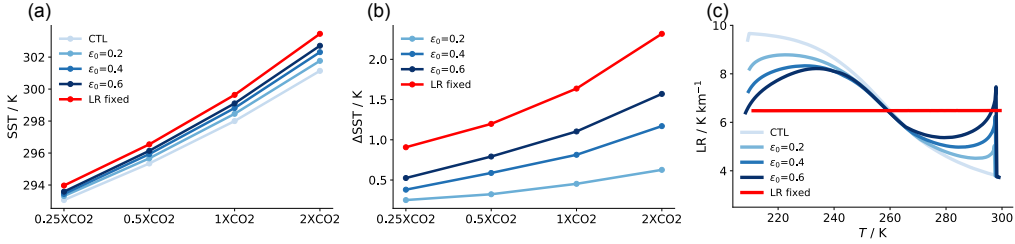


Figure 4. (a) Sea surface temperature (SST) at the equilibrium states as a function of CO₂ concentration. (b) SST changes relative to the control simulations (CTL) as a function of CO₂ concentration. (c) Lapse rate (LR) as a function of atmospheric temperature (T) from simulations of 1×CO₂.

Table 1. Summary of the clear-sky climate sensitivity (\mathcal{S}), forcing ($\Delta F_{2\times\text{CO}_2}$) and feedback (λ).

| Experiments | \mathcal{S}/K | $\Delta F_{2\times\text{CO}_2}/\text{Wm}^{-2}$ | $\lambda/\text{Wm}^{-2}\text{K}^{-1}$ |
|------------------|------------------------|--|---------------------------------------|
| CTL | 3.14 | 4.71 | -1.50 |
| $\epsilon_0=0.2$ | 3.31 | 4.74 | -1.43 |
| $\epsilon_0=0.4$ | 3.49 | 4.80 | -1.37 |
| $\epsilon_0=0.6$ | 3.59 | 4.79 | -1.33 |
| LR fixed | 3.82 | 4.83 | -1.26 |

3 Lapse-rate effects on climate sensitivity

Figure 3b shows the profiles of temperature deviations from the moist-adiabats simulated by konrad. Due to the impact of entrainment, the free troposphere is colder. This cooling effect is increased with a larger entrainment parameter (ϵ_0). The profile simulated by konrad with $\epsilon_0 = 0.2$ best fits the ERA5 profile. Thus, by including a weighted temperature deviation term derived from the zero-buoyancy entraining plume model, our implementation in konrad well captures the main characteristics of the tropical temperature structure.

Figure 4a shows SST in equilibrium from the konrad simulations. In the control simulations which uses a moist-adiabatic adjustment, SST is the lowest, increasing from 293.1 K in 0.25×CO₂ to 301.1 K in 2×CO₂. The highest SSTs occur in simulations with a fixed lapse rate, ranging from 294 K in 0.25×CO₂ to 303.5 K in 2×CO₂. With the impact of entrainment, SST values changes between those from the control simulations and those from simulations with a fixed lapse rate. With the same CO₂ concentration, a stronger entrainment effect (larger ϵ_0) tends to increase SST. Increasing CO₂ concentration further amplifies the surface warming due to entrainment. This is because according to Eq. (3), the impact of entrainment in reducing the temperature is more pronounced in a warmer climate due to the upward shift in the height of convection and also the increase in the saturation deficit that is controlled by the Clausius-Clapeyron relation (Fig. 3c). Thus, our model predicts that even with the same entrainment rate, the temperature deviations from entrainment can lead to more amplified surface warming as CO₂ concentration increases. This extra warming effect will add up to the expected warming from rising CO₂ concentration, promoting an even warmer climate.

With a larger entrainment effect, \mathcal{S} increases consistently from 3.1 K in CTL to 3.6 K in the simulation of $\epsilon_0 = 0.6$ (table 1). This is mainly because of the reduction in λ .

265 In general, cooling in the free troposphere would weaken the lapse-rate feedback. This
 266 is usually balanced by a corresponding decrease in the positive water vapor feedback. How-
 267 ever, as the feedback decreases with stronger entrainment effect, it suggests that the pos-
 268 itive water vapor feedback does not weaken as much to balance the reduction in nega-
 269 tive lapse-rate feedback. This is consistent with Bourdin et al. (2021) who used the same
 270 model and found that the changes in the lapse-rate feedback dominates at low absolute
 271 humidities for a vertically uniform profile of $\text{RH} < 0.75$ at roughly present-day temper-
 272 ature. Due to changes in the effective emission height, perturbing the humidity at dif-
 273 ferent heights in the troposphere can lead to contrasting responses in \mathcal{S} : increasing the
 274 water vapor in the upper troposphere enhances \mathcal{S} , while increasing the water vapor in
 275 the lower mid-troposphere reduces \mathcal{S} (Bourdin et al., 2021). As a result, the total feed-
 276 back change and \mathcal{S} are controlled by the lapse rate change. Indeed, entrainment cool-
 277 ing causes drying in both the upper and lower troposphere. While drying in the upper
 278 troposphere tends to reduce \mathcal{S} , this is compensated, at least partially, by the drying in
 279 the lower troposphere which increases \mathcal{S} . Therefore, the total water vapor feedback change
 280 is moderated. Meanwhile, we find that a larger entrainment effect alters the lapse rate
 281 in a way that more closely resembles a constant lapse rate (Fig. 4c). Therefore, the neg-
 282 ative lapse-rate feedback is weakened and \mathcal{S} is enhanced.

283 Finally, we compare the results from the Atmospheric Model Intercomparison Project
 284 (AMIP) experiments by the models taking part in CMIP6 (Coupled Model Intercom-
 285 parison Project Phase 6; Eyring et al., 2016). We select the data over the period of 2006–
 286 2015 and calculate the tropical mean temperature deviations from moist-adiabats. In
 287 general, CMIP6 models are able to represent the overall temperature deviations from moist-
 288 adiabats, albeit with substantial spread in the free troposphere by individual models (Fig. 3b).
 289 The temperature deviations in CMIP6 are roughly equivalent to those simulated in kon-
 290 rad with ϵ_0 between less than 0.2 and 0.4 in konrad. This would lead to $0.2\text{K} \sim 0.3\text{K}$ spread
 291 in \mathcal{S} . The spread in \mathcal{S} in our simulations is mainly driven by a decrease in λ . Note, that
 292 this change in clear-sky λ could cause a larger spread in all-sky ECS due to the non-linear
 293 dependence of climate sensitivity on the feedback parameter. Hence, the simulated bi-
 294 ases would be expected to contribute to the uncertainties in model estimation of ECS.

295 4 Conclusions

296 We show that the tropical temperature in the free troposphere deviates substan-
 297 tially from a theoretical moist-adiabat in a global storm-resolving model. The overall de-
 298 viations are attributed to the impact of entrainment – the mixing of saturated convective
 299 air parcels with unsaturated environmental air. The temperature deviations approach
 300 zero in the upper troposphere, which we explain with a buoyancy-sorting mechanism:
 301 the height to which individual convective parcels rise depends on its buoyancy, which is
 302 closely tied to how much environmental air it entrains during ascent. While the lower
 303 troposphere, which is easier to reach, is dominated by most of the convection, the up-
 304 per troposphere is increasingly controlled by the convection that is warmer and more buoy-
 305 ant, and is less affected by entrainment.

306 We represent such temperature deviations from moist-adiabats in a clear-sky one-
 307 dimensional RCE model and quantify its impact on the clear-sky climate sensitivity (\mathcal{S}).
 308 The temperature deviation term is represented by weighting the formula derived from
 309 a zero-buoyancy entraining plume model with a height-dependent coefficient. We show
 310 that this idealized representation of entrainment is capable of producing temperature pro-
 311 files more similar to the ERA5 reanalysis. Compared with a strict moist-adiabatic ad-
 312 justment, having this entrainment-induced temperature deviation leads to higher \mathcal{S} , be-
 313 cause entrainment alters the lapse rate in a way that more closely resembles a constant
 314 lapse rate. Notably, as the impact of entrainment depends on the saturation deficit which
 315 increases with warming due to the Clausius-Clapeyron relation, this model predicts even
 316 more amplified surface warming from entrainment in a warmer climate.

317 Although uncertainties in projected warming are largely contributed by the cloud
 318 feedback, this study emphasizes the importance of understanding how the clear-sky feed-
 319 backs change with warming. The CMIP6 model ensemble is capable of replicating the
 320 observed temperature deviations from moist-adiabats. Still, the spread in temperature
 321 deviations among individual models can contribute to the \mathcal{S} uncertainty of $0.2\text{K}\sim 0.3\text{K}$.

322 Entrainment and its impact on lapse rate can potentially influence clouds and cir-
 323 culation which are not represented by our simple model. Results from idealized RCE sim-
 324 ulations show that increased impact of entrainment can lead to more organized convec-
 325 tion (Tompkins & Semie, 2017), and climate sensitivity is associate with changes in the
 326 degree of organization (Becker & Wing, 2020). A recent observational study showed that
 327 deep convective organization modulates tropical radiation budget which is expected to
 328 affect climate sensitivity (Bony et al., 2020). Thus, an improved understanding of the
 329 impact of entrainment on climate sensitivity through clouds and circulation is desired.

330 Acknowledgments

331 The konrad model source code is available on github.com/atmtools/konrad. ERA5 data
 332 (Hersbach et al., 2019) was downloaded from the Copernicus Climate Change Service
 333 (C3S) Climate Data Store ([https://cds.climate.copernicus.eu/cdsapp#!/dataset/
 334 reanalysis-era5-pressure-levels-monthly-means?tab=overview](https://cds.climate.copernicus.eu/cdsapp#!/dataset/reanalysis-era5-pressure-levels-monthly-means?tab=overview)). We thank the
 335 modeling centers for providing the CMIP6 data. The CMIP6 data are made available
 336 for this study by the DKRZ and can be obtained from the ESGF at [https://esgf-data
 337 .dkrz.de/projects/cmip6-dkrz/](https://esgf-data.dkrz.de/projects/cmip6-dkrz/).

338 References

- 339 Bao, J., & Stevens, B. (2021). The elements of the thermodynamic structure of the
 340 tropical atmosphere. *Earth and Space Science Open Archive*. doi: 10.1002/
 341 essoar.10507203.1
- 342 Becker, T., & Wing, A. A. (2020). Understanding the extreme spread in climate
 343 sensitivity within the radiative-convective equilibrium model intercompar-
 344 ison project. *Journal of Advances in Modeling Earth Systems*, 12(10),
 345 e2020MS002165. doi: 10.1029/2020MS002165
- 346 Betts, A. K. (1986). A new convective adjustment scheme. part i: Observational
 347 and theoretical basis. *Quarterly Journal of the Royal Meteorological Society*,
 348 112(473), 677-691. doi: 10.1002/qj.49711247307
- 349 Bony, S., Semie, A., Kramer, R. J., Soden, B., Tompkins, A. M., & Emanuel, K. A.
 350 (2020). Observed modulation of the tropical radiation budget by deep con-
 351 vective organization and lower-tropospheric stability. *AGU Advances*, 1(3),
 352 e2019AV000155. doi: 10.1029/2019AV000155
- 353 Bourdin, S., Kluft, L., & Stevens, B. (2021). Dependence of climate sensitivity
 354 on the given distribution of relative humidity. *Geophysical Research Letters*,
 355 48(8), e2021GL092462. doi: 10.1029/2021GL092462
- 356 Bretherton, C. S., & Smolarkiewicz, P. K. (1989). Gravity waves, compensating sub-
 357 sidence and detrainment around cumulus clouds. *Journal of the Atmospheric
 358 Sciences*, 46(6), 740-759. doi: 10.1175/1520-0469(1989)046<0740:GWCSAD>2.0
 359 .CO;2
- 360 Dacie, S., Kluft, L., Schmidt, H., Stevens, B., Buehler, S. A., Nowack, P. J., ...
 361 Birner, T. (2019). A 1d rce study of factors affecting the tropical tropopause
 362 layer and surface climate. *Journal of Climate*, 32(20), 6769-6782. doi:
 363 10.1175/JCLI-D-18-0778.1
- 364 Eyring, V., Bony, S., Meehl, G. A., Senior, C. A., Stevens, B., Stouffer, R. J., &
 365 Taylor, K. E. (2016). Overview of the coupled model intercomparison project
 366 phase 6 (cmip6) experimental design and organization. *Geoscientific Model
 367 Development*, 9(5), 1937-1958. doi: 10.5194/gmd-9-1937-2016

- 368 Gregory, J. M., Ingram, W. J., Palmer, M. A., Jones, G. S., Stott, P. A., Thorpe,
369 R. B., . . . Williams, K. D. (2004). A new method for diagnosing radiative
370 forcing and climate sensitivity. *Geophysical Research Letters*, *31*(3). doi:
371 10.1029/2003GL018747
- 372 Hersbach, H., Bell, B., Berrisford, P., Biavati, G., Horányi, A., Muñoz Sabater, J.,
373 . . . Thépaut, J.-N. (2019). Era5 monthly averaged data on pressure levels from
374 1979 to present. *Copernicus Climate Change Service (C3S) Climate Data Store*
375 *(CDS)*. (Accessed on 20-DEC-2020). doi: 10.24381/cds.6860a573
- 376 Hohenegger, C., Kornbluh, L., Klocke, D., Becker, T., Cioni, G., Engels, J. F., . . .
377 Stevens, B. (2020). Climate Statistics in Global Simulations of the Atmo-
378 sphere, from 80 to 2.5 km Grid Spacing. *Journal of the Meteorological Society*
379 *of Japan. Ser. II*, *98*(1), 2020–005–91.
- 380 Johnson, R. H., Rickenbach, T. M., Rutledge, S. A., Ciesielski, P. E., & Schubert,
381 W. H. (1999). Trimodal characteristics of tropical convection. *Journal*
382 *of Climate*, *12*(8), 2397 - 2418. doi: 10.1175/1520-0442(1999)012<2397:
383 TCOTC>2.0.CO;2
- 384 Kluft, L., Dacie, S., Buehler, S. A., Schmidt, H., & Stevens, B. (2019). Re-
385 examining the first climate models: Climate sensitivity of a modern radia-
386 tive-convective equilibrium model. *Journal of Climate*, *32*(23), 8111–8125. doi:
387 10.1175/JCLI-D-18-0774.1
- 388 Mapes, B. E. (1993). Gregarious tropical convection. *Journal of the Atmo-*
389 *spheric Sciences*, *50*(13), 2026-2037. doi: 10.1175/1520-0469(1993)050<2026:
390 Gtc>2.0.Co;2
- 391 Mlawer, E. J., Taubman, S. J., Brown, P. D., Iacono, M. J., & Clough, S. A.
392 (1997). Radiative transfer for inhomogeneous atmospheres: Rrtm, a validated
393 correlated-k model for the longwave. *Journal of Geophysical Research: Atmo-*
394 *spheres*, *102*(D14), 16663-16682. doi: <https://doi.org/10.1029/97JD00237>
- 395 Romps, D. M. (2014). An analytical model for tropical relative humidity. *Journal of*
396 *Climate*, *27*(19), 7432-7449. doi: 10.1175/JCLI-D-14-00255.1
- 397 Romps, D. M., & Kuang, Z. (2010). Do undiluted convective plumes exist in the up-
398 per tropical troposphere? *Journal of the Atmospheric Sciences*, *67*(2), 468-484.
399 doi: 10.1175/2009jas3184.1
- 400 Seeley, J. T., & Romps, D. M. (2015). Why does tropical convective available po-
401 tential energy (cape) increase with warming? *Geophysical Research Letters*,
402 *42*(23), 10,429-10,437. doi: 10.1002/2015GL066199
- 403 Singh, M. S., & O’Gorman, P. A. (2013). Influence of entrainment on the ther-
404 mal stratification in simulations of radiative-convective equilibrium. *Geophys-*
405 *ical Research Letters*, *40*(16), 4398-4403. doi: 10.1002/grl.50796
- 406 Singh, M. S., & O’Gorman, P. A. (2015). Increases in moist-convective updraught
407 velocities with warming in radiative-convective equilibrium [Journal Article].
408 *Quarterly Journal of the Royal Meteorological Society*, *141*(692), 2828-2838.
409 doi: 10.1002/qj.2567
- 410 Sobel, A. H., & Bretherton, C. S. (2000). Modeling tropical precipitation in a sin-
411 gle column. *Journal of Climate*, *13*, 4378-4392. doi: 10.1175/1520-0442(2000)
412 013<4378:MTPIAS>2.0.CO;2
- 413 Soden, B. J., & Held, I. M. (2006). An assessment of climate feedbacks in coupled
414 ocean-atmosphere models. *Journal of Climate*, *19*(14), 3354-3360. doi: 10
415 .1175/JCLI3799.1
- 416 Stevens, B., Brogniez, H., Kiemle, C., Lacour, J.-L., Crevoisier, C., & Kiliani,
417 J. (2017). Structure and dynamical influence of water vapor in the lower
418 tropical troposphere. *Surveys in Geophysics*, *38*(6), 1371-1397. doi:
419 10.1007/s10712-017-9420-8
- 420 Tompkins, A. M., & Semie, A. G. (2017). Organization of tropical convection in
421 low vertical wind shears: Role of updraft entrainment. *Journal of Advances in*
422 *Modeling Earth Systems*, *9*(2), 1046-1068. doi: 10.1002/2016MS000802

- 423 Wing, A. A., Reed, K. A., Satoh, M., Stevens, B., Bony, S., & Ohno, T. (2018).
424 Radiative-convective equilibrium model intercomparison project. *Geoscientific*
425 *Model Development*, 11(2), 793-813. doi: 10.5194/gmd-11-793-2018
- 426 Xu, K.-M., & Emanuel, K. A. (1989). Is the tropical atmosphere condition-
427 ally unstable? *Monthly Weather Review*, 117, 1471-1479. doi: 10.1175/
428 1520-0493(1989)117<1471:ITTACU>2.0.CO;2
- 429 Zhou, W., & Xie, S.-P. (2019). A conceptual spectral plume model for understand-
430 ing tropical temperature profile and convective updraft velocities. *Journal of*
431 *the Atmospheric Sciences*, 76(9), 2801-2814. doi: 10.1175/JAS-D-18-0330.1
- 432 Zängl, G., Reinert, D., Rípodas, P., & Baldauf, M. (2015). The icon (icosahedral
433 non-hydrostatic) modelling framework of dwd and mpi-m: Description of the
434 non-hydrostatic dynamical core. *Quarterly Journal of the Royal Meteorological*
435 *Society*, 141(687), 563-579. doi: 10.1002/qj.2378